Accepted Manuscript

An estimation-forecast set-up for iceberg drift prediction ¡!–SPi-PI ¡?xmltex {=0pt=-3pt}?¿ SPi-PI–¿¡!–¡query id="q1"¿Your article is registered as a regular item and is being processed for inclusion in a regular issue of the journal. If this is NOT correct and your article belongs to a Special Issue/Collection please contact michael.evans@elsevier.com immediately prior to returning your corrections.¡/query¿–¿¡!–SPi-PI ¡?xmltex {=0pt=2pc}?¿ SPi-PI–¿¡!–¡query id="q2"¿The author names have been tagged as given names and surnames (surnames are highlighted in teal color). Please confirm if they have been identified correctly.¡/query¿–¿

Leif Erik Andersson, Francesco Scibilia, Lars Imsland

Please cite this article as: Andersson, Leif Erik, Scibilia, Francesco, Imsland, Lars, An estimation-forecast set-up for iceberg drift prediction ¡!–SPi-PI ¡?xmltex {=0pt=-3pt}?¿ SPi-PI–¿¡!–¡query id="q1"¿Your article is registered as a regular item and is being processed for inclusion in a regular issue of the journal. If this is NOT correct and your article belongs to a Special Issue/Collection please contact michael.evans@elsevier.com immediately prior to returning your corrections.¡/query¿–¿¡!–SPi-PI ¡?xmltex {=0pt=2pc}?¿ SPi-PI–¿¡!–¡query id="q2"¿The author names have been tagged as given names and surnames (surnames are highlighted in teal color). Please confirm if they have been identified correctly.¡/query¿–¿, *Cold Regions Science and Technology* (2016), doi: 10.1016/j.coldregions.2016.08.001

An estimation-forecast set-up for iceberg drift prediction ☆

Leif Erik Andersson[a,*], Francesco Scibilia[b], Lars Imsland[a]

[a]*Department of Engineering Cybernetics, Norwegian University of Science and Technology, 7491 Trondheim, Norway*
[b]*Statoil ASA, Statoil Research Center, Arkitekt Ebbells veg 10, 7053 Ranheim, Norway*

Abstract

Iceberg drift forecasting is challenging. Large uncertainties in iceberg geometry and in iceberg driving forces – current, wind and waves – make accurate forecasts difficult. In this work, a new estimation-forecast scheme is proposed that improves iceberg drift forecasts by using past iceberg drift information to reduce uncertainties. Which of the most uncertain parameters to adjust in order to reduce uncertainties, is guided by simple criteria that are introduced and explained. These criteria are applied to different iceberg drift estimation models and a new parameter estimation process is proposed and implemented in the form of a moving horizon estimator. Different performance indices are introduced to evaluate estimation and forecast performance of the proposed set-up. The set-up is tested in a case study on two iceberg drift trajectories surveyed during a research expedition offshore Newfoundland in 2015. The results indicate that the quality of iceberg drift forecasts improve significantly for short-term forecasts, whereas the improvements are smaller for longer forecasts. Moreover, it is demonstrated that the proposed set-up is superior to solutions based on adjustments of the drag coefficients.

Keywords: Iceberg drift forecasting, offshore operations, parameter estimation, moving horizon estimation

1. Introduction

Icebergs are a threat to navigation and offshore installations. Good operational forecasts and risk evaluation are important for marine operations such as station keeping in areas subjected to drifting icebergs. Mechanistic dynamic models, which model the drift of an iceberg by considering the forces that act on the iceberg, were developed by, among others, Smith and Banke (1981); El-Tahan et al. (1983); Bigg et al. (1997). An operational iceberg drift model was developed at the Canadian Ice Service (Kubat et al., 2005). The model uses environmental inputs as wind, waves and currents and detailed description of the iceberg keel geometry to simulate the iceberg trajectory. However, large uncertainties both in environmental driving forces, like current velocities, as well as in iceberg geometry, like the mass and the cross section areas, make the forecast of iceberg movements extremely challenging.

Allison et al. (2014) performed a sensitivity study by creating a base case and varying iceberg model parameters in a range that encompasses 95% of the uncertainty of the parameters. They found that the most important parameter uncertainties are current direction, current speed, wind direction and water drag coefficient. Others also identified currents as most important for the iceberg drift (Kubat et al., 2005; Eik, 2009; Broström et al., 2009; Turnbull et al., 2015).

Smith (1993) tried to hindcast an iceberg drift trajectory by fitting wind and water drag coefficients to one part of the trajectory and applying those parameters to the second part. However, only small improvements were achieved by tuning the drag coefficients. Similar results were obtained by Gaskill and Rochester (1984) and Kubat et al. (2005). Keghouche et al. (2009) found that the drag coefficients become more important for longer periods of 1 to 2 months. In Keghouche (2010), the authors tried to improve iceberg drift hindcast by using an ensemble Kalman filter to update both drag coefficients, which they assumed to account for errors in the estimated vertical cross section area exposed to oceanic and atmospheric forcing.

On the one hand, the main drift direction of dynamic iceberg models is claimed to be satisfactory (Mountain, 1980; Bigg et al., 1997; Kubat et al., 2005), while on the other hand, the modelled and observed trajectories can deviate from the beginning and even point in different directions (El-Tahan et al., 1983). For this reason, Marko et al. (1988) claimed that statistical models have a superior performance for short-term forecasts compared to the dynamic ones. Garrett (1985) and Moore (1987) presented simple statistical methods to predict iceberg motion, while Gaskill and Rochester (1984) used the dynamic iceberg model and past iceberg motions to generate currents required for the past motions. In a second step they applied

those currents to other icebergs passing through the same area at a later time.

Possible large deviations between predicted and actual iceberg trajectories are a threat to operations in areas subjected to drifting icebergs. If an iceberg enters the alert zone, the operation may need to be suspended. The size of the alert zone is based on the rate at which the iceberg approaches the installation and the current state of operation. A mobile offshore drilling unit in exploration drilling can have an alert zone radius of 40 nautical miles. Possible counter-actions to avoid iceberg interaction are iceberg towing or, if active physical ice management is unsuccessful, abort operation and move off location (Randell et al., 2009). Improved iceberg drift prediction facilitates the decision process, improves the safety of human activities and reduces the risk of downtime and possible disconnection.

This article focuses on improving short-term iceberg drift predictions with the help of parameter estimation techniques. Criteria are introduced on how to choose which parameters to update in processes with large uncertainties. With the help of those criteria, different iceberg model options are discussed. Based on the result of this discussion, a moving horizon estimator (MHE) is implemented which estimates the chosen parameters. A case study on real iceberg trajectories measured offshore Newfoundland in spring 2015 illustrates how the proposed estimation scheme can improve short-term iceberg drift predictions.

The article proceeds as follows: In Section 2 the dynamic iceberg model is introduced. Thereafter, criteria are introduced to aid the decision on which components of the iceberg model to estimate in a state and parameter estimation problem. In Section 4, the moving horizon estimator is introduced. In Section 5, the data used in the case study as well as the simulation and estimation set-up is introduced. Section 6 presents the iceberg drift simulation study, which is extended with the parameter estimation study in Section 7. During the estimation study, previously proposed iceberg model adjustments are also performed and compared to the one proposed in this article. The article ends with our conclusion in Section 9.

2. Iceberg drift model

Hereafter the *North-East-Down* (NED) coordinate system is used. Furthermore, the ocean is assumed a plane and the origin of the coordinate system is the initial position of the iceberg. Mechanistic dynamic iceberg models are based on a momentum equation to describe the change of velocity of the iceberg mass

$$m\mathbf{a} = \sum_i \mathbf{F_i}, \qquad (1)$$

where m is the iceberg mass, $\mathbf{a}$ is the acceleration of the iceberg and $\mathbf{F_i}$ are forces acting on the iceberg. Bold symbols are used for three-dimensional vector quantities like

acceleration $\mathbf{a}$ and forces $\mathbf{F_i}$. The approach was already proposed in the seventies (Sodhi and Dempster, 1975) and further developed and evaluated by many different authors, for example (Eik, 2009; Sodhi and El-Tahan, 1980; Smith and Donaldson, 1987; Bigg et al., 1997; Lichey and Hellmer, 2001) and more recently (Turnbull et al., 2015). In this work, it is assumed that the following forces act on the iceberg (Fig. 1)

$$m\mathbf{a} = \mathbf{F_{cor}} + \mathbf{F_a} + \mathbf{F_c} + \mathbf{F_r} + \mathbf{F_p}, \qquad (2)$$

where $\mathbf{F_{cor}}, \mathbf{F_a}, \mathbf{F_c}, \mathbf{F_r}$ and $\mathbf{F_p}$ are the Coriolis force, the air drag force, the water drag force, the wave radiation force and pressure gradient term, respectively. The total mass of the iceberg is m, which consists of the iceberg mass m_0 and added mass m_{add} ($m = m_0 + m_{add} = m_0(1 + C_m)$) due to the water field surrounding the iceberg (Sodhi and El-Tahan, 1980).

The Coriolis force is expressed by

$$\mathbf{F_{cor}} = -m_0 f \mathbf{k} \times \mathbf{V_i}, \qquad (3)$$

where $f = 2\omega sin(\phi)$ is the Coriolis vector, $\mathbf{k}$ is the unit vector directed upwards parallel to the z-axis and V_i is the velocity of the iceberg. The angular velocity of the earth and the latitude of the position of the iceberg is expressed as ω and ϕ. The Coriolis force is caused by rotation of the earth. As a result, moving objects are deflected clockwise on the northern hemisphere.

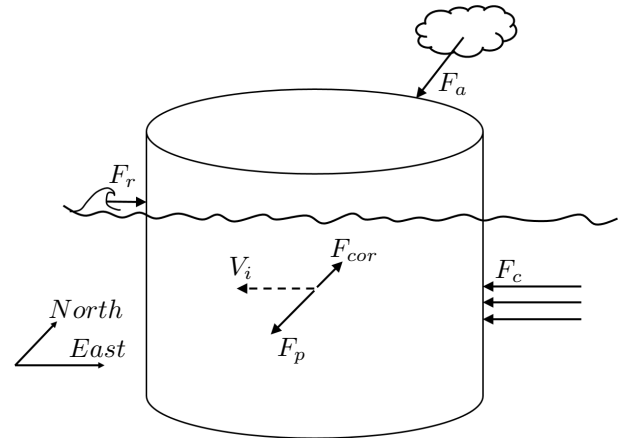The air drag force $\mathbf{F_a}$ is caused by wind acting on the

Figure 1: Forcing on iceberg

iceberg and is given by

$$\mathbf{F_a} = \frac{1}{2}\rho_a C_a A_a |\mathbf{V_a} - \mathbf{V_i}|(\mathbf{V_a} - \mathbf{V_i}), \qquad (4)$$

where ρ_a is the air density, C_a the air drag coefficient, A_a the sail cross section of the iceberg and $\mathbf{V_a}$ the wind velocity. The iceberg velocity $\mathbf{V_i}$ can be typically neglected in Equation (4).

The water drag force $\mathbf{F_c}$ is caused by the current acting

2

on the iceberg and is calculated by

$$\mathbf{F_c} = \frac{1}{2}\rho_c C_w \sum_k A_c(k)|\mathbf{V_c}(k) - \mathbf{V_i}|(\mathbf{V_c}(k) - \mathbf{V_i}), \quad (5)$$

where ρ_c is the water density and C_w is the water drag coefficient. The keel cross section of the iceberg and the current velocity in an underwater layer k is expressed as $A_c(k)$ and $\mathbf{V_c}(k)$. The water column is usually divided into vertical layers of 10 meter height. In this article, we will use a mean current over the keel of the iceberg such that the current is the same in every layer.

The wave radiation force is caused by the waves acting on the iceberg and is calculated as follows:

$$\mathbf{F_r} = \frac{1}{4}C_r \rho_c g a^2 L \frac{\mathbf{V_r}}{\|\mathbf{V_r}\|}, \quad (6)$$

where C_r is the wave drift radiation coefficient, g the gravity, a the wave amplitude, L the characteristic length of the iceberg and $\frac{\mathbf{V_r}}{\|\mathbf{V_r}\|}$ the wave direction.

The pressure gradient in the water causes a force on the iceberg (Kubat et al., 2005), which is approximated by

$$\mathbf{F_p} = m_0 \left(\frac{d}{dt}\mathbf{V_{mc}} + f\mathbf{k} \times \mathbf{V_{mc}} \right), \quad (7)$$

where $\mathbf{V_{mc}}$ is the mean current velocity and f is the Coriolis force parameter.

The characteristic length L of the iceberg is calculated by the equation proposed by Barker et al. (2004)

$$L = \frac{1}{2}(L_0 + \frac{L_0 + W_0}{2}), \quad (8)$$

where L_0 and W_0 are the iceberg waterline length and width respectively. The Cross sectional areas is calculated with the help of L_0 and W_0, the mass is given by

$$m = L_0 W_0 (C_{H_w} H_w + C_{H_a} H_a)\rho_{Ice}, \quad (9)$$

where H_w is the underwater height, H_a is the above water height and C_{H_w} and C_{H_a} are shape coefficients. The iceberg is a cuboid if the shape coefficients are 1.0, whereas the shape coefficients are 0.5 for a triangular shape. Consequently, the iceberg shape can be adapted with the shape coefficients to represent the observed iceberg more accurately. Accurate iceberg shape and mass are not very critical for the later proposed estimation-forecast scheme.

3. Choice of estimated parameters

3.1. Design criteria

An important task in parameter estimation is to analyse the model structure such to find physically reasonable parameters which describe the measured output adequately. The main tool for this is sensitivity analysis (Brun et al., 2001).

The parameters to estimate in the iceberg model should fulfil three important criteria:

1. The model output should be sensitive to changes in the parameters.
2. The estimated parameters should be independent from each other.
3. The parameters should be a physically reasonable representation of the process noise (process noise in this context means non-deterministic inputs, such as modelling errors and external disturbances (Walter and Pronzato, 1997)).

The first criterion ensures that errors in the output can easily be adjusted by changes in the parameters. The second criterion guarantees that the problem is not ill-conditioned, such that changes in one parameter cannot be compensated by appropriate changes in other parameters. The third criterion ensures that the chosen parameters have a reasonable physical interpretation, i.e. that the mechanistic model is not degraded to a black-box model, which just describes the input-output behavior of the process.

3.2. Design criteria applied to the iceberg model

The sensitivity of the model to changes in the environmental forces and to changes in iceberg parameters was investigated earlier by among others Smith and Banke (1983); Kubat et al. (2005); Allison et al. (2014). The results depend on the environmental conditions. However, the current was usually identified as the most influential force on the iceberg. The investigated parameters were air drag coefficient C_a, the water drag coefficient C_w, the wave drift radiation coefficient C_r, the geometric parameters m, L, A_a and A_c as well as the input variables, current, wind and waves.

Smith (1993) and Turnbull et al. (2015) used the air drag and water drag coefficients to tune the iceberg model. Both coefficients were selected in a way that the error between observed and hindcasted iceberg trajectories was minimized. Turnbull et al. (2015) interpreted the results further and categorized based on the optimal drag coefficients whether the icebergs were primarily current or wind-driven. With limited success, Smith (1993) calculated the drag coefficients for one part of the iceberg trajectory and applied those to the second part in order to improve the forecast. The given explanation for the limited success was that the iceberg velocity closely follows the mean water current. For this reason, the water drag force is usually small and therefore the water drag coefficient has limited influence on the iceberg drift. Regarding the air drag coefficient, the explanation was that the wind force is typically of less importance which reflects on the air drag coefficient.

Keghouche (2010) updated both drag coefficients in an ensemble Kalman filter to identify periods when the forcing field was inaccurate. However, the previously introduced criteria are violated if those parameters are chosen

3

to tune the iceberg model. This can be revealed in a simple example.

The air drag force in (Eq. 2) can be written as

$$\mathbf{F_a} = \frac{1}{2}\rho_a C_a A_a |\mathbf{V_a}| \begin{pmatrix} V_a^n \\ V_a^e \\ 0 \end{pmatrix}, \qquad (10)$$

where V_a^n and V_a^e are the wind velocities in north-south and east-west direction. The iceberg velocity is neglected. The Equation (10) can be rewritten as

$$\mathbf{F_a} = \frac{1}{2}\rho_a C_a A_a |\mathbf{V_a}|^2 \begin{pmatrix} \cos(\phi_a) \\ \sin(\phi_a) \\ 0 \end{pmatrix}, \qquad (11)$$

where ϕ_a is the wind direction. This simple conversion shows that the air drag coefficient C_a influences only the first part of Eq. 11 (until brackets) while the second part (vector in brackets) cannot be influenced. Consequently, the air drag coefficient C_a accounts for errors in the absolute wind velocity, sail cross section and air density, but not for errors within the wind direction. Moreover, it should be noted that errors in the absolute velocity are accounted quadratically while errors in the cross section area are accounted linearly. Similar observations can be made for the current, where only the relative velocity between current and iceberg can be corrected, but not directional errors. The change of a single parameter cannot influence the directions. Therefore, both have to be changed to account for directional error. Consequently, the parameters depend on each other. Moreover, a physical interpretation of the estimated parameters is not possible and should be avoided, since wind and drag coefficients have to be adjusted in the same time to correct, for example, directional errors in the current force.

3.3. The ancillary current

The design discussed above can be improved by decomposing the drag coefficient. Considering the current, which has been identified to be the most important driving force, the water drag force can be rewritten as

$$\mathbf{F_c} = \frac{1}{2}\rho_c A_c |\mathbf{V_{mc}} - \mathbf{V_i}| \begin{pmatrix} C_w^n(V_{mc}^n - V_i^n) \\ C_w^e(V_{mc}^e - V_i^e) \\ 0 \end{pmatrix}, \qquad (12)$$

where C_w^n and C_w^e are the decomposed water drag coefficients and $\mathbf{V_{mc}}$ is the mean current in the water column over the iceberg keel. A second option is to correct the current directly with two current coefficients C_w^{e*} and C_w^{n*}

$$\mathbf{F_c} = \frac{1}{2}\rho_c A_c |\mathbf{V_{mc}} - \mathbf{V_i}| \begin{pmatrix} (C_w^{n*}V_{mc}^n - V_i^n) \\ (C_w^{e*}V_{mc}^e - V_i^e) \\ 0 \end{pmatrix}. \qquad (13)$$

However, both designs violate the first design criterion. In the first case, the model becomes insensitive to changes of

the water drag coefficients if the iceberg velocity is close to the current velocity. In the second case, the model becomes insensitive and even singularities occur if the current velocity in one of the directions becomes zero. An example of this estimation process from the case study in Section 5 is shown in Fig. 2. Large values and short time excitations of the current coefficients in situations of low current velocities in one or both directions make this design not suitable for use in short-term forecasts.

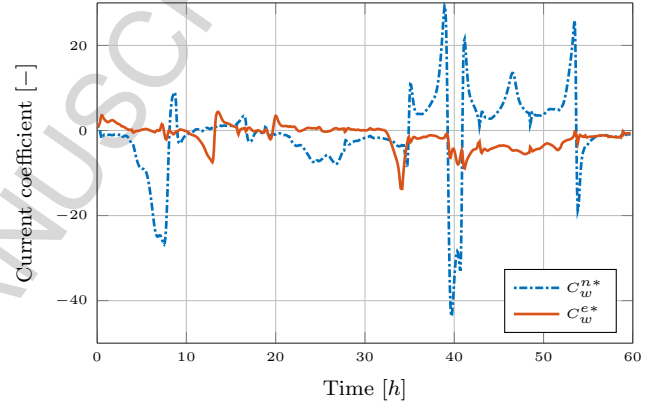In order to avoid singularities and to be able to account

Figure 2: Estimation of current coefficients

for large uncertainties, this work proposes to estimate instead an artificial current that we denote *ancillary current*. This ancillary current is added to the measured/predicted current in the model to correct for the observed iceberg drift trajectory. The water drag force is rewritten as

$$\mathbf{F_c} = \frac{1}{2}\rho_c A_c C_w |(\mathbf{V_{mc}} + \mathbf{V_c^*}) - \mathbf{V_i}| \begin{pmatrix} (V_{mc}^n + V_c^{n*}) - V_i^n \\ (V_{mc}^e + V_c^{e*}) - V_i^e \\ 0 \end{pmatrix},$$
$$(14)$$

where V_c^{n*} and V_c^{e*} are the directional decomposed ancillary current. The ancillary current can correct directional and absolute velocity errors in the current force. The process noise, like uncertainties in environmental driving forces and geometrical uncertainties, are collected and corrected with the ancillary current. Since the current has the largest uncertainty, it is beneficial to correct the current with the estimated variable. Thus, this new design fulfils all three criteria.

4. MOVING HORIZON ESTIMATOR

The mechanistic dynamic system from Section 2 can be described by a set of ordinary differential equations (ODEs)

$$\dot{x}(t) = \tilde{f}(x(t), u(t)), \quad x_0 = x(t_0), \qquad (15a)$$
$$y(t) = h(x(t)), \qquad (15b)$$

4

where $x \in \mathbb{R}^{n_x}$ is the vector of differential states, $u \in \mathbb{R}^{n_u}$ the vector of inputs, and $y \in \mathbb{R}^{n_y}$ the vector of outputs. For example in the iceberg model, x can be iceberg position, velocity (and ancillary current), u current and wind forecast and y iceberg position. Discretizing the continuous time model yields

$$x_{k+1} = f(x_k, u_k) + w_k, \quad x_0 = x(t_0), \qquad (16a)$$
$$y_k = h(x_k) + v_k, \qquad (16b)$$

in which k denotes the samples taken at discrete time t_k. The vector $w_k \in \mathbb{R}^{n_x}$ is additive process noise, which accounts for unknown disturbances on the system states. The measurement noise $v_k \in \mathbb{R}^{n_y}$ is added to the measured outputs. The MHE for the above model is an optimization problem (Robertson et al., 1996):

$$\min_{\{x_i, w_i, v_i\}} \|\hat{x}_M - x_M\|_{P^{-1}}^2 + \sum_{i=M}^{N} \|v_i\|_{R^{-1}}^2 + \sum_{i=M}^{N-1} \|w_i\|_{Q^{-1}}^2$$
$$(17a)$$

$$s.t. \quad x_{i+1} = f(x_i, u_i) + w_i \quad \forall i = M, ..., N-1$$
$$y_i = h(x_i) + v_i \qquad \forall i = M, ..., N \qquad (17b)$$
$$x_i \in \mathbb{X}, \ w_i \in \mathbb{W}, \ v_i \in \mathbb{V},$$

where $P \in \mathbb{R}^{n_x \times n_x}$ is the estimated error covariance matrix, $R \in \mathbb{R}^{n_y \times n_y}$ the measurement noise covariance matrix and $Q \in \mathbb{R}^{n_x \times n_x}$ the process noise covariance matrix. The vector $\hat{x}$ represents the estimated vector. The matrices Q and R are tuning parameters. In addition to their statistical interpretation, the matrix Q can be seen as a measure of confidence in the model equations and the matrix R as a measure of confidence in the process data (Scibilia and Hovd, 2009). The horizon contains $(N - M + 1)$ measurements, taken at times $t_{k=M} < ... < t_{k=N}$. The sets $\mathbb{X}$, $\mathbb{W}$ and $\mathbb{V}$ are closed and convex, and usually, they are finite dimensional polyhedral sets

$$\mathbb{X} = \{x_i \in \mathbb{R}^{n_x} | D_x x_i \le d_x\},$$
$$\mathbb{W} = \{w_i \in \mathbb{R}^{n_x} | D_w w_i \le d_w\}, \qquad (18)$$
$$\mathbb{V} = \{v_i \in \mathbb{R}^{n_y} | D_v v_i \le d_v\},$$

where $D_x \in \mathbb{R}^{n_x \times n_x}$, $D_w \in \mathbb{R}^{n_x \times n_x}$ and $D_v \in \mathbb{R}^{n_y \times n_y}$ are matrices. The MHE formulation is a constrained least-squares problem. Optimization variables are x_i, w_i and v_i, which represent the state, the process noise and the measurement noise vector in the optimization horizon. The variable space of the optimization problem can be reduced by substitution to initial state x_M and the process noise $\{w_i\}_{i=M}^{N-1}$ over the optimization horizon. The arrival cost term is represented by $\|\hat{x} - x_M\|_{P^{-1}}^2$, which summarizes past data $(t < t_{k=M})$ that is not explicitly part of the present objective function. The arrival cost is key to stability of the MHE, is derived from dynamic programming arguments and typically uses Kalman filter based updates

(Kühl et al., 2011). The optimal estimate of x_M is denoted by $\hat{x}_M$. The arrival cost is updated with the update scheme developed by Tenny and Rawlings (2002). The MHE is chosen in this work, since it provides improved state estimation and greater robustness to both poor guesses of the initial state and tuning parameters compared to the extended Kalman filter (EKF) (Haseltine and Rawlings, 2005).

The performance of the MHE will be compared with that of a standard EKF. In order to obtain the state estimates, the EKF linearizes the non-linear system around the last filter estimate and then applies the Kalman filter (Rawlings and Bakshi, 2006). With the following linearization

$$F_k = \left.\frac{\partial f_k}{\partial x}\right|_{\hat{x}_k^+}, \qquad H_k = \left.\frac{\partial h_k}{\partial x}\right|_{\hat{x}_k^-}, \qquad (19)$$

the method can be summarized in a recursion with time update

$$\hat{x}_{k+1}^- = f(\hat{x}_k^+, u_k), \qquad (20a)$$
$$P_{k+1}^- = F_k P_k^+ F_k^T + Q, \qquad (20b)$$

where the minus sign represents the a priori time update and the plus sign the a posteriori measurement update. In a second step, the measurement update is performed and the mean and covariance are given by

$$K_k = P_k^- H_k^T \left(H_k P_k^- H_k^T + R\right)^{-1}, \qquad (21a)$$
$$\hat{x}_k^+ = \hat{x}_k^- + K_k \left[y_k - h(\hat{x}_k^-)\right] \qquad (21b)$$
$$P_k^+ = (I - K_k H_k) P_k^-, \qquad (21c)$$

where Q and R are again the process and measurement noise covariances.

5. Data acquisition and preparation of iceberg drift simulation & estimation (case study)

5.1. Data acquisition

The iceberg trajectories used in this case study were measured during the Offshore Newfoundland Research Expedition conducted by ArcticNet (ArcticNet, 2004-2016) and Statoil in spring 2015.

The two studied icebergs, Iceberg 1 and Iceberg 2, are a dry dock and an eroded dome-shaped iceberg (Fig. 3). A dry-dock is an eroded iceberg forming a large u-shape slot with twin columns or pinnacles. The slot may extend under the waterline, which is the case for Iceberg 1. A dome-shape iceberg is categorised by a smooth rounded top (McClintock et al., 2002). Large irregular shapes of icebergs make the simulation of iceberg drift more difficult. The sea ice concentration, indicated as the ratio of sea area covered by sea ice to total area (WMO, 1970), is in both cases less than 3/10 and composed by relatively small ice floes. It is assumed that the sea ice concentration has minor influence on the iceberg drift. Consequently, the

(a) Iceberg 1 - dry dock

(b) Iceberg 2 - dome-shaped

Figure 3: Two iceberg studied during the Offshore Newfoundland Research Expedition 2015
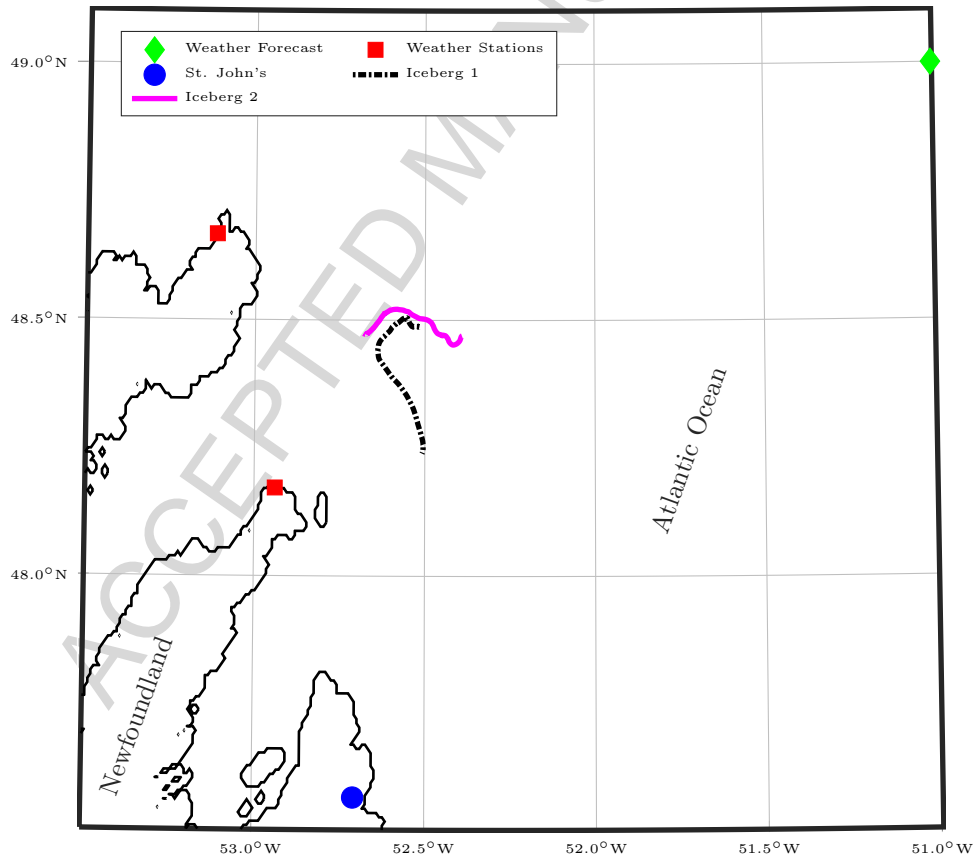

Figure 4: Location point for the ordered weather forecasts (Forecast), the weather stations located in Bonavista and Grates Cove (Weather stations), the two icebergs trajectories (Iceberg 1 and Iceberg 2), and the city of St. John's

sea ice force is neglected in simulations.

Both icebergs were discovered close to St. John's. On both icebergs a Canatec GPS tracker was deployed, which has an accuracy of 1.8 m and measured the position of the icebergs with a five minutes frequency. Fig. 4 shows the recorded iceberg trajectories, the location point for which

the weather forecast by Amec Foster Wheeler was ordered, and the two local weather stations at Bonavista and Grates Cove.

When the ship was close to the iceberg the sail height of the first iceberg was measured by triangulation to be approximately 30 m. The length of the first iceberg was

(a) SVP

(b) SLDMB

Figure 5: The MetOcean SVP and SLDMB buoys

estimated to be 210 m and the width to be 150 m. As the ship-mounted SX90 sonar measured the iceberg keel depth to be between 45 m and 60 m, it was here taken as 55 m. The sail height of the second iceberg was estimated to be about 16.5 m and the length and width to be 100 m. The keel depth was measured to be around 75 m. The total water depth at the iceberg locations is about 200 m.

Two current drifters deployed close to each iceberg collected current information, one MetOcean Iridium surface velocity program buoy (SVP) with a 15 m drogue and one MetOcean Iridium self-locating data marking buoy (SLDMB), which measured the surface current (Fig. 5). Position updates from the SVP were received with an hourly frequency, while SLDMB position updates were received with a ten minutes frequency. Both measurements were interpolated in simulations to fit the time stamp of the position data of the iceberg.

Both current drifters measured similar current velocities at Iceberg 1. At Iceberg 2, the data of the SVP drifter was not received and consequently only the surface current data of the SLDMB drifter is available for simulations. Thus, during simulations and estimations for Iceberg 1, the 15 m current information from the SVP drifter is used, and for Iceberg 2 the surface current information from the SLDMB drifter is used. Since deeper currents were not measured, the overall current force on the iceberg keel is uncertain. Wind and wave information was obtained by a weather forecast provided twice a day by Amec Foster Wheeler. The forecast time step was 6 h. In order to have values in between the time steps the wind and wave information was interpolated to fit the data points of the iceberg position. The weather forecast and initial iceberg positions are around 110–125 km apart (Fig. 4). Additional wind information was received by two weather stations 30–60 km apart from the iceberg positions. Predicted wind at the forecast location and measured wind at the two weather stations are similar with respect to velocity and direction (Fig. 6).
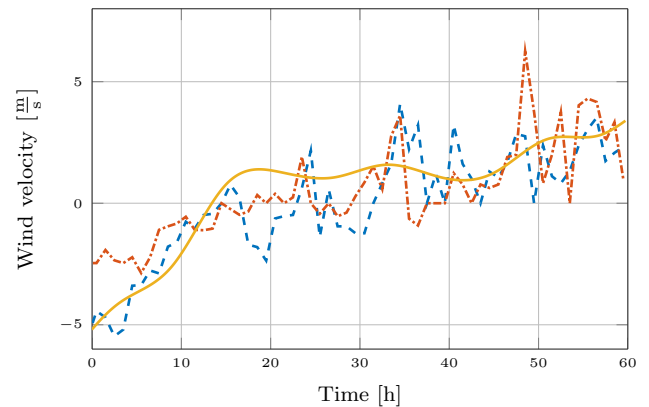
(a) North - South
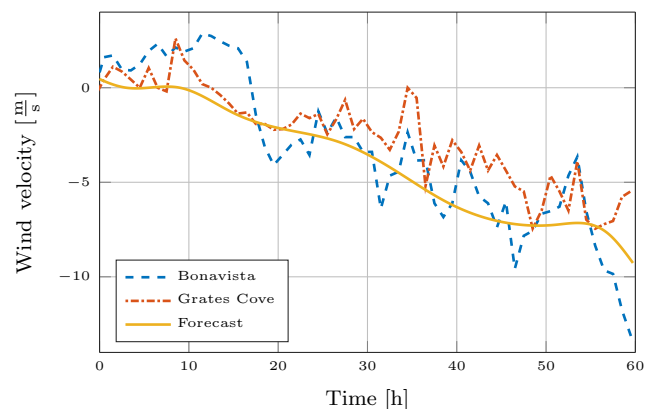
(b) East - West

Figure 6: Predicted and measured wind velocity in both directions. The location of the weather stations is illustrated in Fig. 4, where the station further north is Bonavista.

7

5.2. Simulation & estimation set-up

The shape coefficients C_{H_w} and C_{H_a} are chosen to be 0.6 and 0.15 for Iceberg 1 and 0.8 and 0.8 for Iceberg 2. The dry-dock sail shape factor is taken from Rudkin et al. (2005), whereas the others are guessed based on the geometry of the iceberg and the assumed ratio between keel and sail cross-section. The air drag coefficient C_a and water drag coefficient C_w are selected to be 1.3 and 0.9 (Eik, 2009). Water, air and ice densities are fixed to be 1027, 1.225 and $900 \, \mathrm{kg \, m^{-3}}$. The added mass coefficient C_m is assumed to be 0.5 (Eik, 2009).

During the observation of the icebergs, the significant wave height did not exceed 1.5 m and was most of the time less than 0.5 m. Such small waves can be neglected, since they have only a minor influence on the iceberg drift.

The states x of the dynamic system are the iceberg position and iceberg velocity. In addition, the state vector is augmented with the ancillary current. Thus, the estimation model has six states and four inputs u, which are the current and wind velocity. The measured output is the iceberg position.

The initial iceberg velocity is not known and assumed zero. Consequently, the initial state for the MHE is

$$x_0 = [0, 0, 0, 0, 0, 0]^T, \qquad (22)$$

where the first two states represent the iceberg position, the next two the iceberg velocity and the last two the ancillary current. The iceberg position is given in m, whereas the iceberg velocity and ancillary current is given in m/s. The iceberg certainly moved when the GPS was deployed. However, the error introduced by the assumption of zero initial iceberg velocity is small for simulations longer than 1–2 h. In addition, the error is corrected by the estimator. The initial error covariance is chosen to be

$$P_0 = diag(1, 1, 1, 1)^2, \qquad (23)$$

the measurement noise covariance is

$$R = diag(20, 20)^2, \qquad (24)$$

and the process noise covariance is

$$Q = diag(3 \cdot 10^{-6}, 3 \cdot 10^{-6}, 6 \cdot 10^{-6}, 6 \cdot 10^{-6}, 6 \cdot 10^{-5}, 6 \cdot 10^{-5})^2. \qquad (25)$$

The covariances are chosen in a way such that model uncertainties are largely corrected with changes in the ancillary current. The states of the process are estimated for the first 60 h after the surface drifters were deployed. If not stated otherwise, the horizon length of the MHE is chosen to be 24 h. The MHE performance in the iceberg drift case shows little sensitivity to changes in the horizon size. Nevertheless, slight improvements can be detected with increasing horizon size. The MHE problem is implemented in the Python programming language and solved by using the open-source software tool CASADI (Andersson et al., 2012). The software package IPOPT is used as

solver for the non-linear program (Wächter and Biegler, 2006). The computational burden is not a limitation, as the optimization can be solved on a personal computer in less than a second for the proposed horizon length.

6. Simulation Study

The iceberg trajectories are simulated in the simulation study by using the iceberg drift model with constant parameters. The icebergs initial position is the first measured GPS position and the wind input is taken from the weather forecast.

6.1. Iceberg 1

The simulated Iceberg 1 diverges immediately from the measured iceberg trajectory (Fig. 7). The real iceberg drifts first towards the west, it follows for a period of 25 h approximately the underwater contour lines, before it changes drift direction and drifts towards south-east. The simulated iceberg drifts first south-westwards, makes a half circle to the east, and drifts afterwards the westwards, towards the coastline. The coastline does not represent an active constraint in the simulation model; therefore, it is possible that simulated iceberg trajectories drift on land regions. This can be avoided by grounding the iceberg and stopping the simulation when the iceberg enters shallow water regions close to the coastline. Both measured current and predicted winds are directed approximately to the west. Consequently, those forces cannot explain the real iceberg trajectory. The influence of the wind force within the observation horizon is weak because the wind velocity is relatively small. The simulated iceberg trajectories change only slightly if wind measured at the weather stations is used (Fig. 7: grey lines).

6.2. Iceberg 2

The simulated iceberg trajectories of Iceberg 2 also diverge immediately from the measured iceberg trajectory (Fig. 8). The divergence is even stronger than for Iceberg 1. The real iceberg drifts westward, while the simulated iceberg trajectory drifts southwards the first 6 h and south-eastwards the nest 24 h. Thereafter, it makes a turn and drifts westwards. The mean velocity of the simulated iceberg is twice as high as of the observed iceberg. Consequently, the overall trajectory of the simulated iceberg is twice as long as the one of the real iceberg. The use of measured winds from the weather stations changes only insignificantly the simulated iceberg trajectory compared to the iceberg trajectory where forecasted wind is used (Fig. 8: grey lines).

The simulated trajectory of Iceberg 2 can be improved by the current measurements of the SVP current drifter deployed at Iceberg 1 (Fig. 9). The same observation can be obtained if the data of the SLDMB current drifter deployed at Iceberg 1 is used. Iceberg 1 and 2 are about
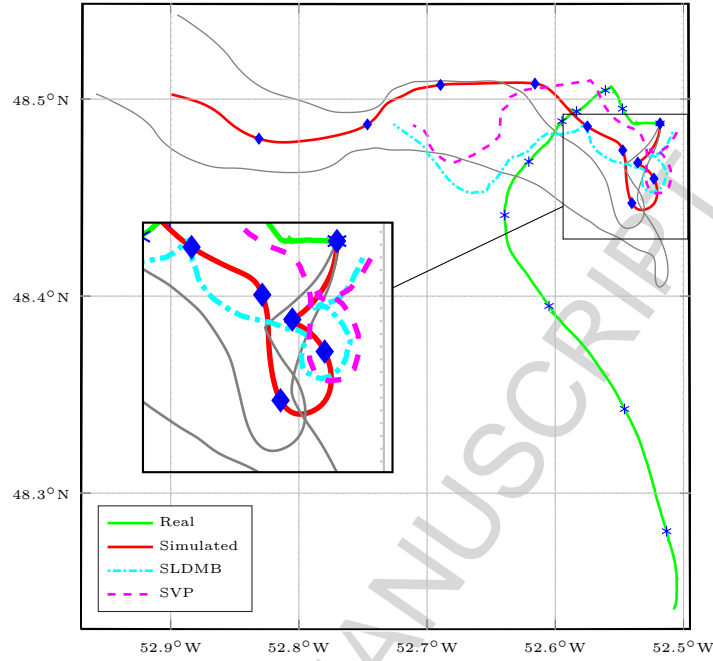
8

Figure 7: GPS measured (green) and simulated (red) Iceberg 1 trajectories as well as SLDMB and SVP drifter trajectories. Every 6 h a mark is set in the measured and simulated trajectories. The grey lines show the simulated iceberg trajectories when wind measured by the weather stations is used.
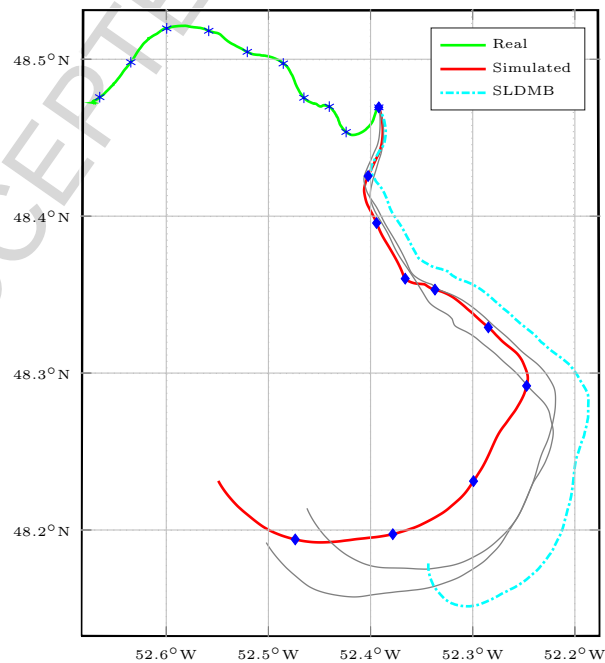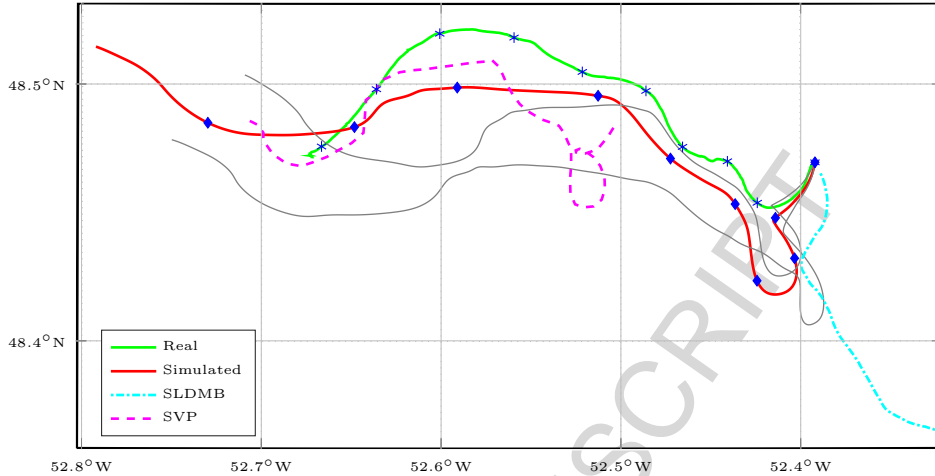

Figure 8: GPS measured (green) and with $SLDMB$ current simulated (red) Iceberg 2 trajectories as well as SLDMB drifter trajectories. Every 6 h a mark is set in the measured and simulated trajectories. The grey lines show the simulated iceberg trajectories when wind measured by the weather stations is used.

9

Figure 9: GPS measured (green) and with SVP current simulated (red) Iceberg 2 trajectories as well as SLDMB and SVP drifter trajectories. Every 6 h a mark is set in the measured and simulated trajectories. Grey lines show simulated iceberg trajectories if wind measured by the weather stations is used.

9 km apart from each other at the beginning of the observations. It is, therefore, reasonable to assume that currents (15 m or surface current) provide a better proxy for current in the water column at Iceberg 2 than the surface current measured at Iceberg 2. In addition, the distance between SVP drifter and Iceberg 2 shortly after initialization is smaller than the distance between SLDMB drifter deployed at Iceberg 2 and Iceberg 2. The overall direction of the iceberg trajectory is simulated correctly. However, there exists some discrepancy in time and place between observed and simulated iceberg trajectory. The simulated iceberg trajectory describes a half circle at the beginning of the simulation. Such a behaviour cannot be observed for the real trajectory. As a consequence, the simulated iceberg trajectory has a delay of about 6 h to the observed trajectory. At the end of the observation horizon, a higher simulated iceberg velocity due to upcoming wind balances the delay. For this reason, the simulated and observed iceberg trajectories are only 860 m apart from each other after 54 h.

6.3. Discussion

The simulation study shows that the overall influence of wind measurements is small. This is a consequence of strong similarities between wind measurements and forecast, but surely also due to relatively weak winds during the observations. In contrast, the influence of the measured current is strong in the simulations. The measured surface or near-surface currents at the two icebergs differ significantly, even though the initial positions are close to each other. The simulations of the two icebergs with current measured at both icebergs do not correlate well with the observed iceberg trajectories. However, the measured currents are surface or near-surface currents, which are

mainly wind driven and do not represent the whole current in the water column of the iceberg keel. Hence, it can be concluded that for iceberg drift simulations only surface current information is not enough and may even lead to erroneous forecasts. An improvement in the simulated trajectories of Iceberg 2 can be observed if the currents measured at Iceberg 1 are used in simulations. Consequently, it can be assumed that the current measured at Iceberg 1 is a better overall representation of the current at Iceberg 2 than the surface current measured at Iceberg 2. In order to further improve simulation and prediction with the given information it is necessary to update/adjust parameters in the iceberg model.

7. Estimation study

If the measured and predicted forcing does not agree with the actual iceberg trajectory, it is important to use the available information to correct the forcing within the operational iceberg model to improve the simulation and forecast results. One may say that the ideal drifter to estimate the forcing on the iceberg is the iceberg itself. The estimation-forecast procedure is envisioned as follows (Fig. 10): In an MHE smoothing scheme, the measurements are used to estimate the state vector of the iceberg model. The state vector contains iceberg position, velocity and ancillary current. This state vector x_0 is given as initial condition to the forecast, which performs a forward simulation of the iceberg model. During the forecast the position and velocity of the iceberg changes with time, while the ancillary current is constant. This procedure is repeated as new measurements are received.

In the analysis it is assumed that the surface current measurements are available during the forecast. Current
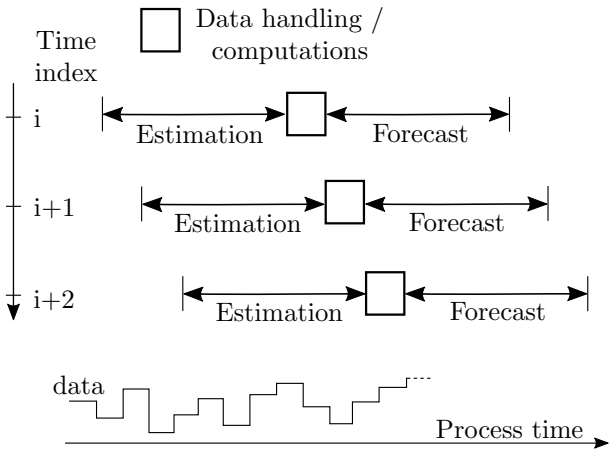
10

Figure 10: Estimation and forecast procedure with MHE

measurements are typically unavailable for operational iceberg drift forecasts, therefore current forecasts are used more often instead. If the time-varying ancillary current were known a priori, it would be possible to predict almost perfectly the iceberg drift trajectory. However, the ancillary current is not known a priori, but it is estimated as new measurements are received.

7.1. Forecast Performance Indices

In order to quantify the performance of the forecast at a specific time, the square root of mean squared distance between predicted X_{pred} and measured X_{meas} iceberg trajectory is calculated

$$\zeta_N(t) = \sqrt{\frac{1}{N} \sum_{i=1}^{N} \|X_{pred}(t+i) - X_{measured}(t+i)\|_2^2},$$
(26)

where N is the length of the forecast period and t is the initial time of the forecast. The performance index (PI) for the whole observation horizon is the root mean square of ζ_N (Eq. 26) with the same forecast horizon N

$$PI(N) = \sqrt{\frac{1}{M} \sum_{i=1}^{M} \zeta_N(t_i)^2},$$
(27)

where M is the number of forecasts performed and t_i is the initial time of the forecast.
A discrepancy measurement between modelled and observed iceberg trajectories is the absolute velocity of the ancillary current. An overall discrepancy index (DI) is the root mean square of all calculated absolute velocities of ancillary currents

$$DI(N) = \sqrt{\frac{1}{M} \sum_{i=1}^{M} \|V_c^*(t_i)\|_2^2}.$$
(28)

In this article, the most recently estimated ancillary current is used as ancillary current vector over the whole forecast horizon. The assumption is, therefore, that the ancillary current does not change during the prediction. As new measurements of the iceberg trajectory are received, the estimated ancillary current is updated and a new forecast is initialized. The overall forecast error is caused by discrepancy in the forecasted wind and current inputs as well as other model errors. However, the ancillary current gives a numerical value to the discrepancy in the iceberg model. Therefore, the difference between a new estimated (actual) ancillary current $\hat{V}_c^*$ and the previously assumed (forecasted) ancillary current $\bar{V}_c^*$ indicates the magnitude of the prediction error. This observation leads directly to the ancillary current performance index (API), which is strongly correlated with the average distance ζ_N (Eq. 26)

$$API(t) = \sqrt{\frac{1}{N} \sum_{i=1}^{N} \left\| \bar{V}_c^*(t+i) - \hat{V}_c^*(t+i) \right\|_2^2}.$$
(29)

While the average distance ζ_N gives the outcome of the forecast, the API provides more an explanation for the error of the prediction. The advantage of evaluating the forecast performance with the API, is that the average distance ζ_N can be directly influenced by the assumed ancillary current vector $\bar{V}_c^*$. The assumed ancillary current $\bar{V}_c^*$ is an input to the forecast model and it is assumed constant during the forecast in this paper. However, other options like linearly decreasing or clockwise rotating ancillary currents could be used for forecasting iceberg trajectories. The API represents a direct measure to evaluate those options.

The root mean square of all $APIs$ is the *ancillary current performance prediction index* (APPI)

$$APPI(N) = \sqrt{\frac{1}{M} \sum_{i=1}^{M} API(t_m)^2}.$$
(30)

The $APPI$ is similar to the PI and gives an overall reason for the discrepancy in the forecasts.

7.2. Iceberg 1
7.2.1. Estimation of ancillary current

The ancillary current for Iceberg 1 is shown in Fig. 11. Small, consistently changing oscillations can be observed within the estimated ancillary current. Significant direction changes are detected around hour 15 and 38. An almost constant ancillary current is observed from the hours 20 to 35. If the ancillary current evolution was known a priori and used in simulation, the iceberg trajectory of Iceberg 1 could be almost perfectly simulated (Fig. 12). The difference between observed and simulated iceberg trajectory can be further reduced by tuning (selecting other process and measurement noise parameters). However, doing this may influence numerical conditioning of the MHE.
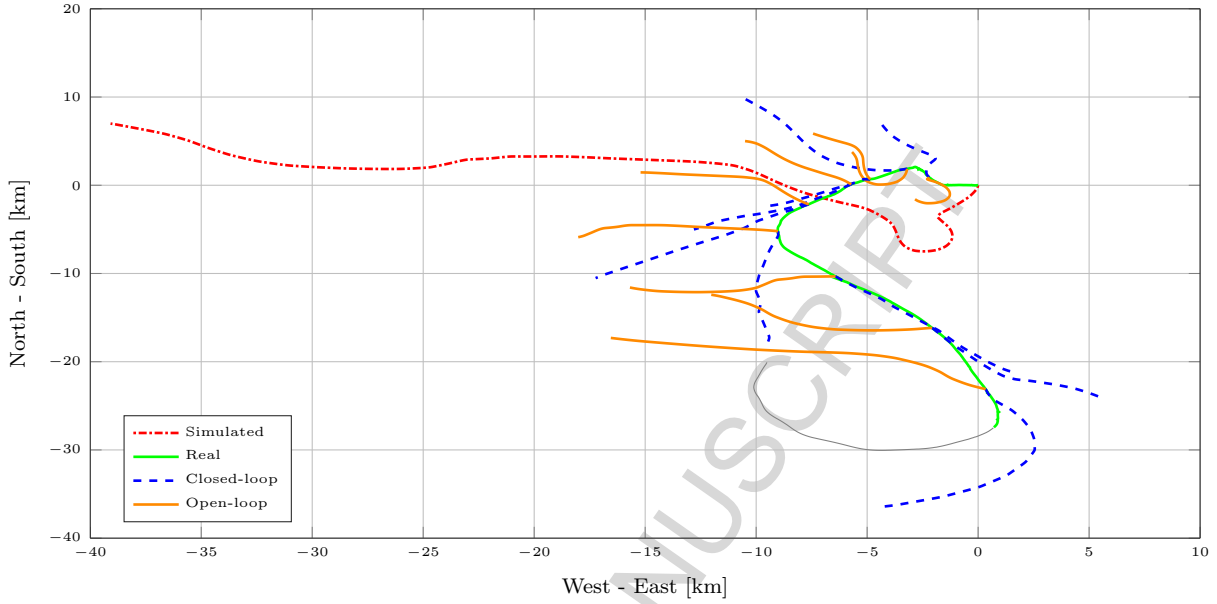
11

Figure 13: Closed-loop (blue) and open-loop (orange) 12 h predictions in 6 h intervals of Iceberg 1. The reference trajectories are the simulated iceberg trajectory (dotted) and the measured iceberg trajectory (solid). The grey line shows the measured iceberg drift for the first 12 h after the 60 h observation horizon.
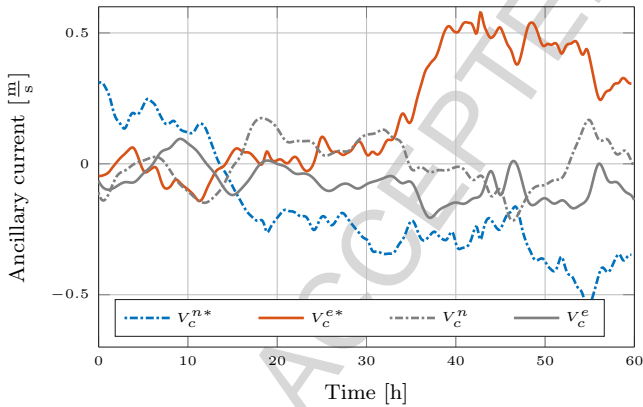

Figure 11: The ancillary current calculated with an MHE smoothing scheme and the measured SVP current for Iceberg 1.

Figure 12: GPS measured (green) and simulated iceberg trajectory without ancillary current (red) as well as with ancillary current known a priori (blue) of Iceberg 1.

7.2.2. Forecast of iceberg trajectory with the help of the estimated ancillary current

In Fig. 13, several 12 h iceberg drift predictions with and without the use of the ancillary current are illustrated. The iceberg trajectories predicted with calculated ancillary current (indicated as closed-loop) are compared with the trajectories forecasted without using the ancillary current (indicated as open-loop, since no feedback from esti-

mates is used)[1]. In open-loop, the iceberg drift model is

---

[1] The terminology *open-loop* and *closed-loop* is frequently used in process system engineering for control loops with feedback (closed-

reinitialised at the last measured iceberg position. The results indicate higher prediction performance by using the ancillary current. The improvement is especially substantial in the first few hours (short time horizons). For forecasts over longer horizons, the assumption of constant ancillary current over the forecast horizon is less correct and prediction performance decreases. However, significant improvements are noted if the ancillary current is almost constant over the forecast horizon (hour 20–35).

It should be emphasized that the use of ancillary current allows the prediction of wind induced direction changes, as it can be seen at the end of the observation horizon. Strong winds cause a clockwise loop, which is approximately predicted by the ancillary current set-up (last forecasted trajectory of closed-loop in Fig. 13).

The square root of mean squared distance between predicted and measured iceberg trajectory calculated with (Eq. 26) decreases significantly in the closed-loop case (Fig. 14). Closed-loop predictions show considerably better performance compared to open-loop prediction in the short time forecasts (~ 1 h). The prediction error in closed-loop is reduced by 95 %. A reason for the significant improvement is the almost constant ancillary current within a short time period. Consequently, the correction, performed by the ancillary current, remains almost constant and an almost correct current force is applied during the forecast. If the ancillary current is used for longer time predictions, the square root of mean squared distance (Eq. 26) can be larger in the closed-loop case than in the open-loop case ($\sim$ hour 12 in Fig. 14b). Those periods correspond to periods of strong changes in estimated ancillary current. Hence, the offset between predicted input forces and real forces, which is adapted with the help of ancillary current, changes. Nevertheless, the overall averaged prediction performance improves significantly in closed-loop. In addition, the predicted direction of the iceberg drift is correct at the beginning of each forecast.

In order to obtain the performance of the forecast for a specific horizon, the PIs (Eq. 27) are calculated for different prediction horizons. In closed-loop, the PI reduces about 80 % in a six-hour forecast and about 70 % in a twelve-hour forecast. Even in a 24 h-forecast, the PI is reduced about 50 % (Table 1).

If improved information about the input forces is used,

Table 1: The PI (Eq. 27) of Iceberg 1 for different prediction horizons N.

Horizon N [h]	1	3	6	12	24
Open-loop [m]	809	2399	4819	9799	20020
Closed-loop [m]	40	308	1026	3315	9723

(a) N = 1 hour

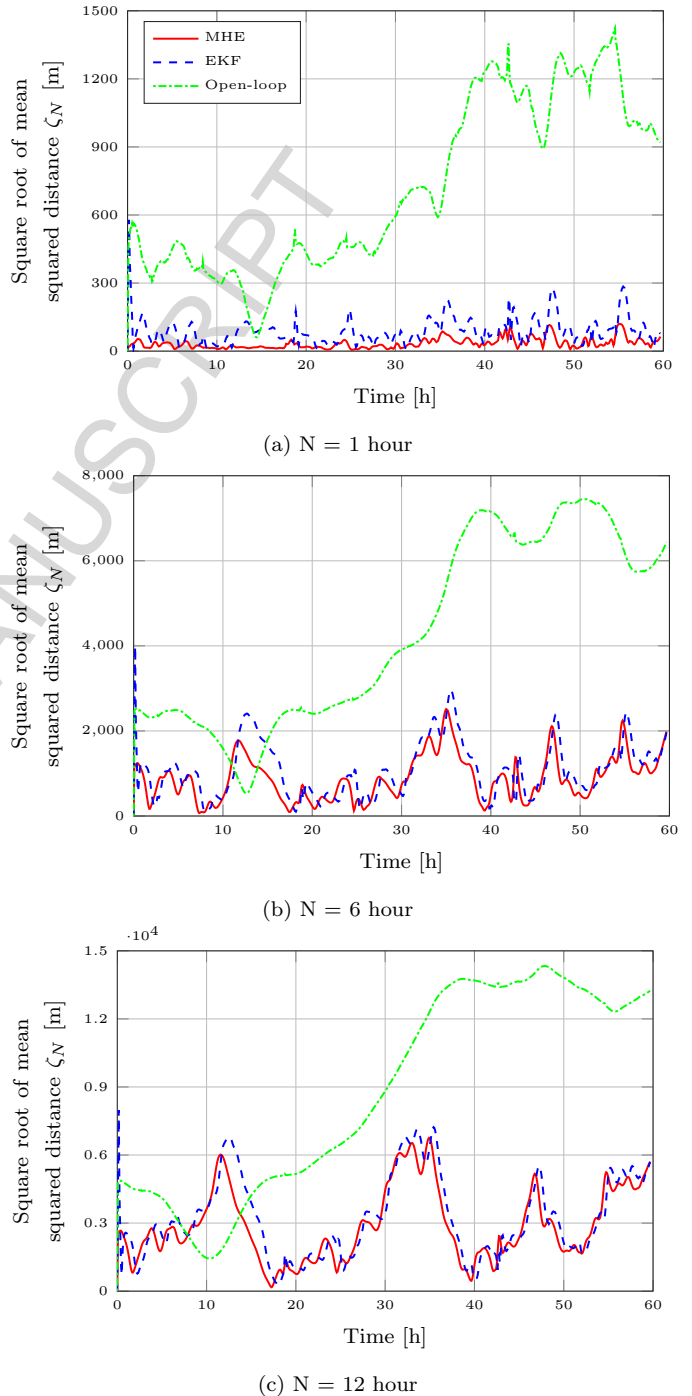(b) N = 6 hour

(c) N = 12 hour

Figure 14: The square root of mean squared distance (Eq. 26) of closed-loop and open-loop case of Iceberg 1 are compared for different forecast horizons N. The ancillary current was calculated with a MHE and an EKF.

as for example the measured wind at the weather stations, the forecast will in general benefit from it. This applies especially for longer forecasts. For instance, in closed-loop

13

the PI is for a 12 h forecast with forecasted wind 3315 m. This can be improved to 3060 m by using only measured wind data (during estimation and forecast). However, the measured wind is not available during forecasts. If, instead, forecasted wind is used during forecast and measured wind during estimation, the PI decreases to 3643 m. The differences in this example are relative small since the predicted and measured winds are similar. A change of input information between estimation and forecast step is not recommended, since it is detrimental to the forecast quality when estimating the ancillary current. The ancillary current is calculated for a specific combination of input forces to the model and it corrects for this input set-up. A change of the input set-up in the forecast will change the process noise, which is approximately represented by the ancillary current.

7.3. Iceberg 2

7.3.1. Estimation of ancillary current

Fig. 15 shows the ancillary current for Iceberg 2 when the SLDMB surface current measurements at Iceberg 2 are used. The northern component experiences a significant change around hour 42. The eastern component experiences two small changes around hour 10 and 25 and a large change, similar to Iceberg 1, around hour 35. As already stated for Iceberg 1, it is expected that the forecast will especially improve in areas outside of large changes of ancillary current.
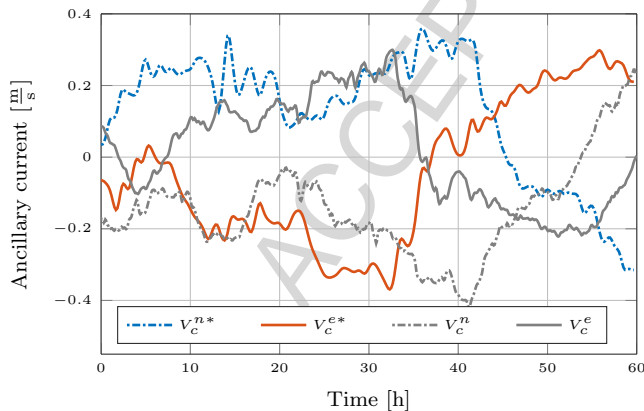
Figure 15: The ancillary current calculated with an MHE smoothing scheme and the measured SLDMB current for Iceberg 2.

7.3.2. Forecast of iceberg trajectory with the help of estimated ancillary current

Fig. 16 displays a 12 h prediction in closed-loop and open-loop every 6 h. The closed-loop set-up prevents the predicted iceberg trajectories from having wrong directions at the beginning of the prediction, as it happens

in the open-loop case. However, it is not guaranteed to be correct over a longer forecast horizon. It can happen that after already a relative short period the applied ancillary current is not correct any more and the predicted trajectory diverges from the observed one.

For example, variations in the predicted current in relation to the real current in one time step to the other change simultaneously the process (input) noise. Thus in such situations, the assumption of constant ancillary current is not correct and it will decrease the forecast quality. between closed-loop and open-loop case of Iceberg 2 are compared s N. The ancillary current was calculated with a MHE and an EKF, and the SLDMB current was used as current input. For longer forecast horizons, this can cause a lower forecast accuracy with ancillary current than without (Fig. 17c: Hour 42). However, those situations are not common. Hence, the PI (27) of the forecast with ancillary current is superior to the one without (Tab. 2).

The forecast of Iceberg 2 can be significantly improved

Table 2: The PI (Eq. 27) of Iceberg 2 for different prediction horizons N, when $SLDMB$ current is used in the forecasts.

Horizon N [h]	1	3	6	12	24
Open-loop [m]	606	1801	3589	7104	13801
Closed-loop [m]	36	295	1053	3678	11831

if the measured SVP current at Iceberg 1 are used instead of the measured SLDMB surface current at Iceberg 2, as discussed in Section 6.2, cf. Fig. 8 and 9. The ancillary current indicates well which input combination is most suitable, since it represents a factor of discrepancy between modelled and observed iceberg trajectories. Fig. 18a shows the ancillary current estimated for Iceberg 2 when the SVP current measurements of Iceberg 1 are used. In addition, the absolute ancillary current of the SVP case (dashed red line) and SLDMB case (solid black line) is shown in Fig. 18b. The absolute ancillary current with SVP current is most of the time lower than the ancillary current with SLDMB current. The DI (Eq. 28) for the case with SLDMB current is $0.2936\,\mathrm{m\,s^{-1}}$ and with SVP current $0.1521\,\mathrm{m\,s^{-1}}$. This indicates that the SVP current is superior to the SLDMB current for open-loop simulations of Iceberg 2. However, the improvement in closed-loop is by far smaller than for the open-loop case (Tab. 3 in comparison to Tab. 2). While in open-loop the PI approximately halves for all prediction horizons, the improvements in closed-loop for short-term forecasts are small and increase only for longer forecasts (longer than 6 h). Again, this observation is connected to the parameter estimation scheme presented here. It is expected that the estimated ancillary current is able to compensate for poor
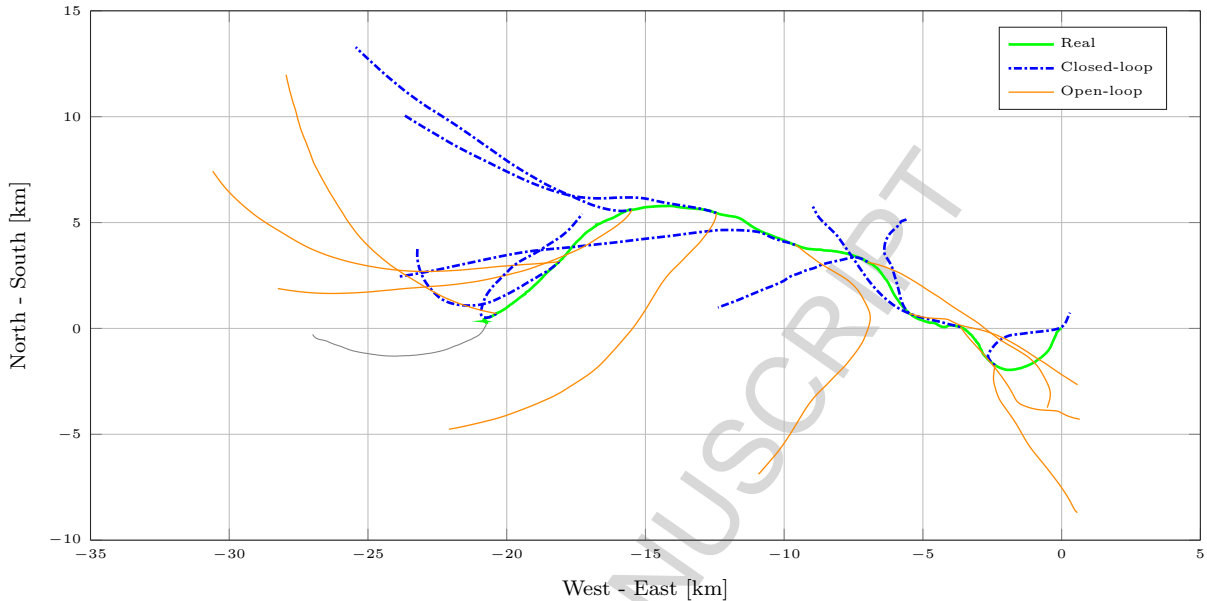
Figure 16: Closed-loop (blue) and open-loop (orange) 12 h prediction in 6 h intervals of Iceberg 2. The reference trajectory is the measured iceberg trajectory (solid). The grey line shows the measured iceberg drift for the first 12 h after the 60 h observation horizon.

Table 3: The PI (Eq. 27) of Iceberg 2 for different prediction horizons N, when SVP current is used in the forecasts

Horizon N [h]	1	3	6	12	24
Open-loop [m]	314	955	2042	4818	10521
Closed-loop [m]	40	302	949	2897	7001

quality input for short enough forecasts. Therefore, the prediction of the iceberg trajectory with the help of the ancillary current will be in a certain range from the real drift, which is defined by the maximum possible change of ancillary current within the prediction horizon. This motivated the introduction of the API (Eq. 29). Fig. 19 shows the API for two forecast horizons for both considered input combinations of Iceberg 2. The square root mean squared distance ζ_N (Eq. 26) in Fig. 17c and the API_{SLDMB} in Fig. 19b have a similar evolution, since both values are strongly connected to each other. The API for a 1 h forecast (Fig. 19a) shows strong oscillations and sudden changes. Both $APIs$ are comparable in magnitude. The $APPI$ for the one hour forecast is 0.0469 m/s with SLDMB current and 0.0462 m/s with SVP current. Both values are similar as expected, since the PI is also very similar (Tab. 2 and 3). However, for longer predictions the $APPI$ is significant lower for the SVP case (12 h: SVP

$= 0.1298\,\mathrm{m\,s^{-1}}$, SLDMB $= 0.2144\,\mathrm{m\,s^{-1}}$), which indicates in average a better performance of the SVP case. However, there are periods where the SLDMB case is superior to the SVP case. Those periods correlate to periods where the API of the SLDMB case is smaller than the one of the SVP case.

7.4. Comparison between chosen design and estimation of air and water drag coefficient

In order to validate the discussion in Section 3, air and water drag coefficients are estimated with the MHE and EKF instead of the ancillary current. The coefficients are constrained between [0.01, 2.5], which are physically reasonable values for the coefficients (Turnbull et al., 2015).

7.4.1. Iceberg 1

The value of the estimated drag coefficients are both at the lower boundary of 0.01 for most of the time (Fig. 20).

The performance of the forecast decreases significantly, even though some improvement compared to the open-loop case can be observed (Tab. 4 and Fig. 21). The performance decrease is explained by a low sensitivity of the model output to changes of the water and air drag coefficients (Sec. 3.2).

Without constraints on the drag coefficients, a similar performance as with the ancillary current can be achieved in a 1 h forecast. However, the performance decreases significantly for longer prediction horizons. In addition, nega-

(a) N = 1 hour

(b) N = 6 hour

(c) N = 12 hour
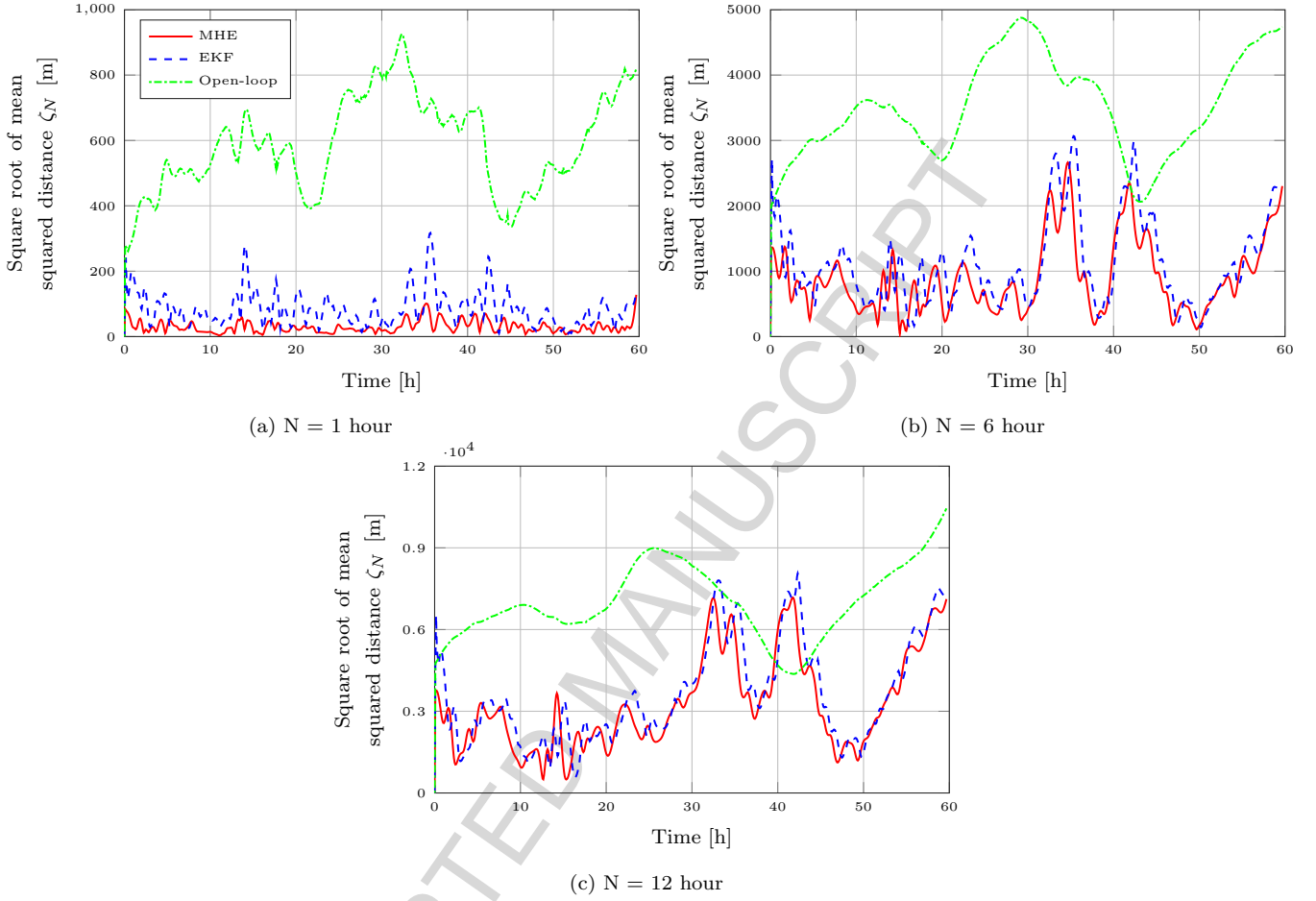
Figure 17: The square root of mean squared distance (Eq. 26) between closed-loop and open-loop case of Iceberg 2 are compared for different forecast horizons N. The ancillary current was calculated with a MHE and an EKF, and as current input the SLDMB current was used.
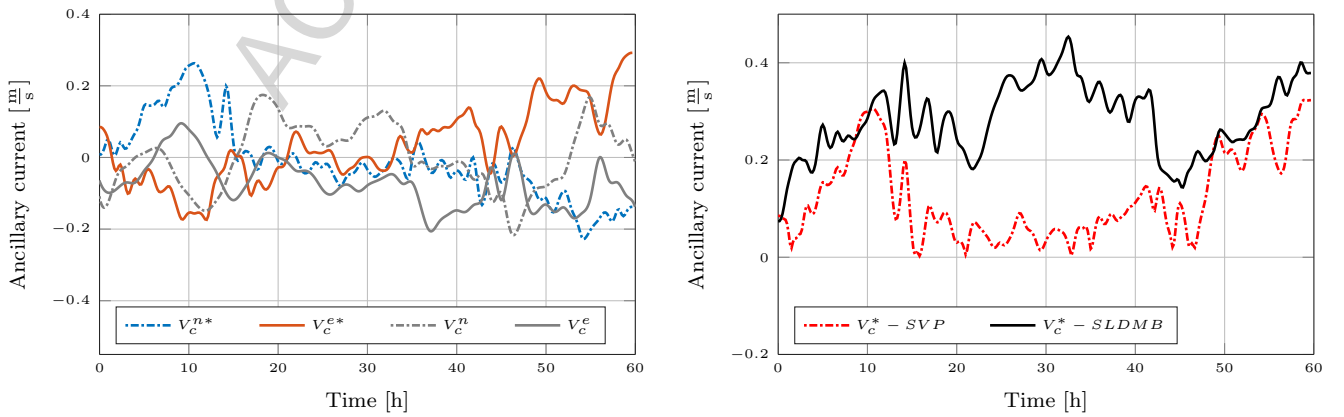

(a) The ancillary current when SVP current at Iceberg 1 is used. The grey lines show the measured current.

(b) Absolute ancillary current of SVP case (dashed red) and SLDMB case (solid black).

Figure 18: Ancillary current calculated with a MHE smoothing scheme for Iceberg 2 with SVP current.

16

(a) N = 1 hour

(b) N = 12 hour
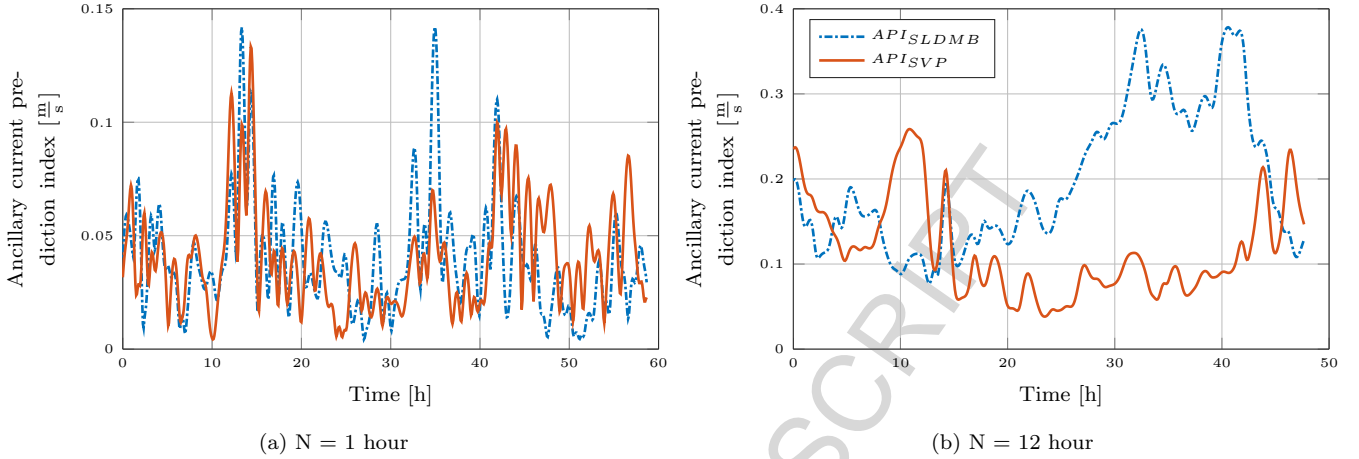
Figure 19: The *API* for prediction of trajectory of Iceberg 2 with SLDMB current and SVP current for different prediction horizons
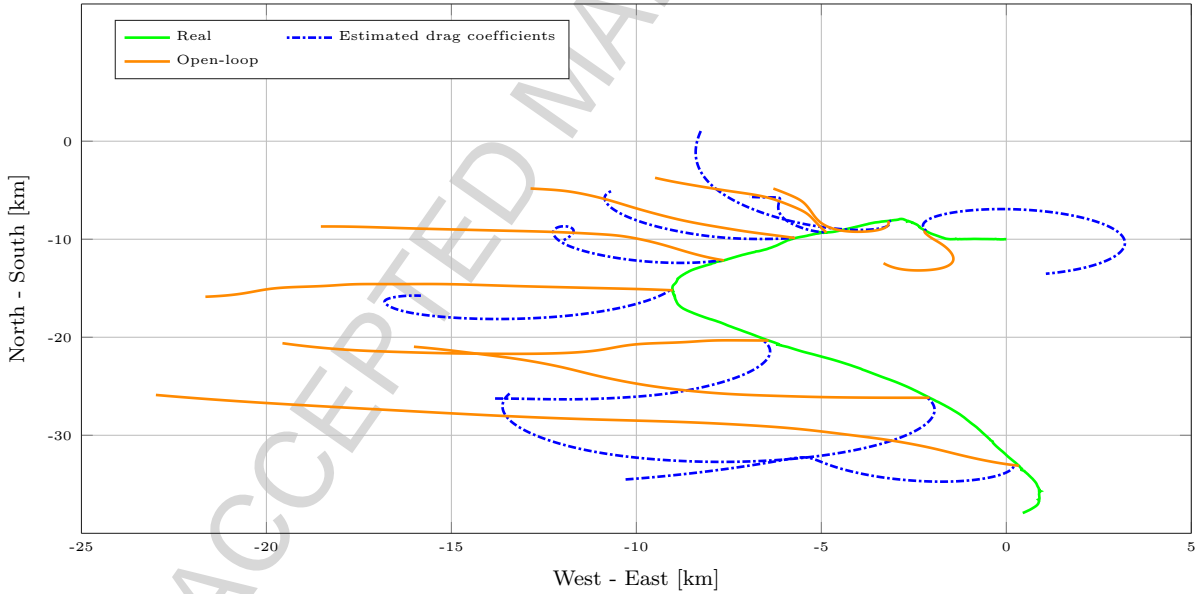
Figure 21: Twelve hour forecasts with estimated drag coefficients (blue) and open-loop (orange). Reference trajectory is the measured iceberg trajectory (solid)

Table 4: The *PI* (Eq. 27) in 1, 6 and 12 h forecast with estimated drag coefficients

Horizon [h]	1	6	12
PI [m]	305	3013	7040
Reference (Tab. 1)			
PI - Open-loop [m]	809	4819	9799
PI - Closed-loop [m]	40	1026	3315

tive values for the drag coefficients can be obtained, which is non-physical.

7.4.2. Iceberg 2

Fig. 22 shows the MHE and EKF results for the drag coefficients of Iceberg 2 when the SVP current of Iceberg 1 is used as current input.

Constraints can be easier and more directly included in the MHE than in the EKF calculations. Furthermore, when estimating drag coefficients the estimation model is more non-linear. Non-linearities can be better handled by the MHE than by the EKF. For these reasons, the two estimators have larger differences when drag coefficients
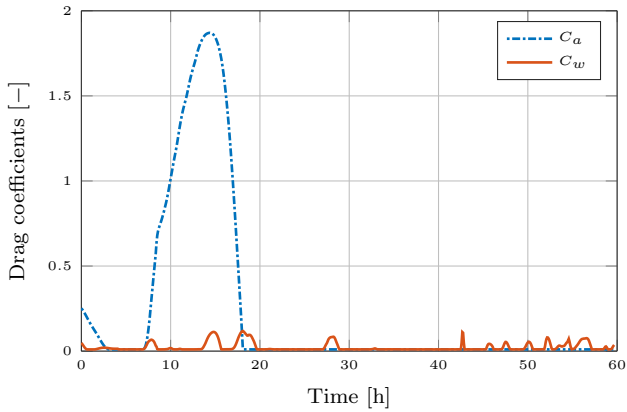
Figure 20: Estimated drag coefficients for Iceberg 1
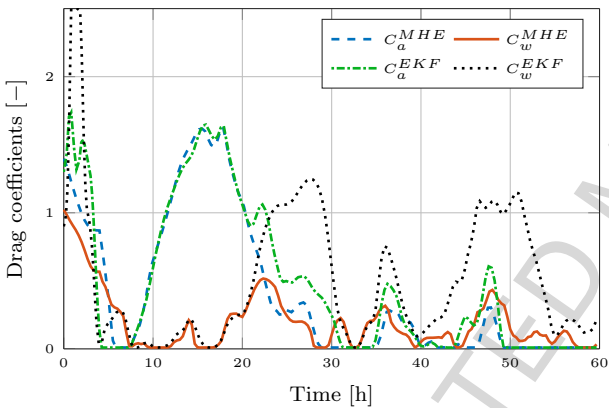
Figure 22: Estimated drag coefficients using MHE and EKF for Iceberg 2 with SVP current

are estimated than in the case when ancillary currents are estimated.

During the 60 h observation, the average values of the MHE calculated air and water drag coefficients are $C_a =$ 0.41 and $C_w = 0.20$, while the EKF calculates average values of $C_a = 0.48$ and $C_w = 0.51$. The larger difference between both estimators in water drag is also caused by larger non-linearities of the water drag force compared to the air drag force.

Fig. 23 shows the drag coefficients for Iceberg 2 where the SLDMB current of Iceberg 2 is used. The average air drag is $C_a = 1.19$ and the average water drag is $C_w = 0.05$.

The difference between the calculated drag coefficients with SVP current (Fig. 22) and with SLDMB current (Fig. 23) is large. However, the interpretation of the estimated drag coefficients is difficult. They do not reflect a specific characteristic of the iceberg itself but of the used input forces. The air drag coefficient is on the upper boundary from hour 16 to hour 38, while the water drag coefficient is small. This may indicate that during this period the wind
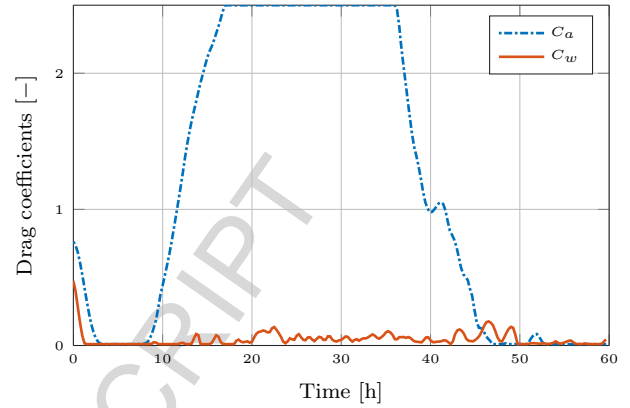
Figure 23: Estimated drag coefficients for Iceberg 2 with SLDMB current

force is more strongly prioritised by the prediction scheme to explain the iceberg motion. Nonetheless, it cannot be concluded that the iceberg is mainly wind-driven, since the overall wind force on the iceberg is still small. Instead, it can be deduced that the iceberg is current-driven, but the current input is wrong. As a consequence, it is beneficial for the optimizer to reduce this wrong force and amplify another to reduce the error.

8. Discussion

In the estimation study, the ancillary current is estimated for two icebergs. The square root of mean squared distance ζ_N, represented by the PI, can be reduced by using the ancillary current for both icebergs compared to the open-loop case. The ancillary current allows increasing significantly the accuracy of the prediction of the iceberg trajectory in short forecasts. Moreover, improvements for longer forecasts can also be observed. However, it should be emphasised that the open-loop case using only the near surface currents is a low standard against which to evaluate the closed-loop model. Measured current profiles or current forecasts from ocean models, the latter is often available during offshore operations, would probably improve the quality of the used input information, and may reduce the improvements offered by the closed-loop model.

It is illustrated that improved input information will ultimately lead to an improved forecast. However, one should use consistent (the same type of) inputs in the estimation and forecast process, since the estimated ancillary current corrects errors in the inputs that are used in the estimation process. Furthermore, it is illustrated how the ancillary current can be used to evaluate different input sources. For example, if two different wind forecasts are available the one with the smallest absolute ancillary current represents best the real wind situation at the iceberg and will most probably also generate the best open-loop forecast. However, this cannot be guaranteed over the

whole forecast horizon.

The ancillary current can be a good tool to compare different current inputs. Furthermore, the ancillary current may be a good starting point for investigating whether available current information is useful for the iceberg forecast. A large ancillary current can indicate that the current information is error-prone and that it should be excluded from the forecast.

The forecast quality by use of ancillary current, on the other hand, is strongly correlated with the *API* and the *APPI*. These indices express on the one hand the change of discrepancy between simulated and observed iceberg trajectory and on the other hand they can be used to evaluate directly different options of predicted ancillary current trajectories used in the forecast.

An important observation for the forecast with ancillary current is that the ancillary current can correct the overall discrepancy between real iceberg and observed iceberg caused, for example, by erroneous inputs. Such biased inputs are not only observed when surface drifters are used but also, for example, in current forecasts from ocean models (Eik, 2009). As long as the discrepancy stays the same, the assumption of constant ancillary current is correct and the forecast scheme produces good quality forecasts.

The approach of estimating an ancillary current is compared to estimation of drag coefficients, which has been suggested in previous works. The adjustment of drag coefficients improved the forecast marginally and significantly less than using ancillary current. Moreover, the physical meaning of the estimated drag coefficients is lost and interpretations should be done with care.

9. Conclusion

This article proposed the concept of an estimated ancillary current to correct for discrepancy between observed and simulated iceberg trajectories. It was discussed why an added current force is superior to other possible corrections, like correction of the drag coefficients. A case study was performed and the proposed correction scheme was tested on two real iceberg trajectories. In both cases, the forcing on the iceberg and the iceberg geometry were uncertain and produced large discrepancies between predicted and actual iceberg trajectories in simulations. Suitable performance indices were introduced to give numerical values for the uncertainties in the forcing on the iceberg, as well as for the forecast performance.

The ancillary current is a suitable variable to express the process noise and can correct for discrepancy between simulated and observed iceberg trajectories. The calculation of the ancillary current was performed by an optimization-based MHE. It was shown that a similar performance can be achieved with less complicated estimators, like the EKF. However, that is a trade-off between performance and complexity.

It was shown that the iceberg forecast can be improved with the help of the ancillary current. The improvement

was especially large in short-term forecast or in cases when the discrepancy was almost constant. However, the improvement usually decreased for longer predictions horizons. The relative improvement by using the ancillary current was large in the two case studies, since the input forces were to a high degree uncertain and erroneous. It is believed that the improved forecast performance with the proposed set-up will carry over to other cases, for example, where measured current profiles or currents from ocean models are used.

Acknowledgement

References

Allison, K., Crocker, G., Tran, H., Carrieres, T., 2014. An ensemble forecast model of iceberg drift. Cold Regions Science and Technology 108, 1 – 9.

Andersson, J., Åkesson, J., Diehl, M., 2012. Casadi: a symbolic package for automatic differentiation and optimal control. In: Recent Advances in Algorithmic Differentiation. Springer, pp. 297–307.

ArcticNet, 2004-2016. [Online]. Available: www.arcticnet.ulaval.ca.

Barker, A., Sayed, M., Carrieres, T., 2004. Determination of iceberg draft, mass and cross-sectional areas. In: Proc. International Offshore and Polar Engineering Conference'04. Vol. 2. pp. 899–904.

Bigg, G. R., Wadley, M. R., Stevens, D. P., Johnson, J. A., 1997. Modelling the dynamics and thermodynamics of icebergs. Cold Regions Science and Technology 26 (2), 113–135.

Broström, G., Melsom, A., Sayed, M., Kubat, I., Dec. 2009. Iceberg modeling at met.no: Validation of iceberg model. Tech. Rep. 17, Norwegian Meteorological Institute.

Brun, R., Reichert, P., Künsch, H. R., 2001. Practical identifiability analysis of large environmental simulation models. Water Resources Research 37 (4), 1015–1030.

EI-Tahan, M., EI-Tahan, H., Venkatesh, S., et al., 1983. Forecast of iceberg ensemble drift. In: Offshore Technology Conference.

Eik, K., 2009. Iceberg drift modelling and validation of applied metocean hindcast data. Cold Regions Science and Technology 57, 67–90.

Garrett, C., 1985. Statistical prediction of iceberg trajectories. Cold Regions Science and Technology 11 (3), 255 – 266.

Gaskill, H. S., Rochester, J., 1984. A new technique for iceberg drift prediction. Cold Regions Science and Technology 8 (3), 223 – 234.

Haseltine, E. L., Rawlings, J. B., 2005. Critical evaluation of extended kalman filtering and moving-horizon estimation. Industrial & engineering chemistry research 44 (8), 2451–2460.

Keghouche, I., Aug. 2010. Modeling the dynamics and drift of icebergs in the barents sea. Ph.D. thesis, University of Bergen.

Keghouche, I., Bertino, L., Lisæter, K. A., 2009. Parameterization of an iceberg drift model in the barents sea. Journal of Atmospheric and Oceanic Technology 26 (10), 2216–2227.

Kubat, I., Sayed, M., Savage, S. B., Carrieres, T., 2005. An operational model of iceberg drift. International Journal of Offshore and Polar Engineering 15 (2), 125–131.

Kühl, P., Diehl, M., Kraus, T., Schlöder, J. P., Bock, H. G., 2011. A real-time algorithm for moving horizon state and parameter estimation. Computers & Chemical Engineering 35 (1), 71–83.

Lichey, C., Hellmer, H. H., 2001. Modeling giant-iceberg drift under the influence of sea ice in the weddell sea, antarctica. Journal of Glaciology 47 (158), 452–460.

Marko, J., Fissel, D., Miller, J., 1988. Iceberg movement prediction off the canadian east coast. In: El-Sabh, M., Murty, T. (Eds.), Natural and Man-Made Hazards. Springer Netherlands, pp. 435–462.

McClintock, J., Bullock, T., McKenna, R., Ralph, F., Brown, R., 2002. Greenland iceberg management: Implications for grand banks management systems. PERD/CHC Report 20-65, AMEC Earth & Enviromental and C-Core, St. John's, NL.

Moore, M., 1987. Exponential smoothing to predict iceberg trajectories. Cold Regions Science and Technology 14 (3), 263 – 272.

Mountain, D., 1980. On predicting iceberg drift. Cold Regions Science and Technology 1 (3-4), 273 – 282.

Randell, C., Ralph, F., Power, D., Stuckey, P., et al., May 2009. Ss: Canadian: Atlantic development; technological advances to assess manage and reduce ice risk in northern developments. In: Proc. Offshore Technology Conference. Houston, TX.

Rawlings, J. B., Bakshi, B. R., 2006. Particle filtering and moving horizon estimation. Computers & Chemical Engineering 30 (10-12), 1529–1541.

Robertson, D. G., Lee, J. H., Rawlings, J. B., 1996. A moving horizon-based approach for least-squares estimation. AIChE Journal 42 (8), 2209–2224.

Rudkin, P., Boldrick, C., Barron Jr, P., 2005. Perd iceberg management database. PERD/CHC Report, 20–72.

Scibilia, F., Hovd, M., 2009. Multi-rate moving horizon estimation with erroneous infrequent measurements recovery. In: Fault Detection, Supervision and Safety of Technical Processes. pp. 1037–1042.

Smith, S. D., 1993. Hindcasting iceberg drift using current profiles and winds. Cold Regions Science and Technology 22 (1), 33–45.

Smith, S. D., Banke, E., 1981. A numerical model of iceberg drift. In: Proc. Port and Ocean Engineering under Arctic Conditions'81.

Smith, S. D., Banke, E., 1983. The influence of winds, currents and towing forces on the drift of icebergs. Cold Regions Science and Technology 6 (3), 241–255.

Smith, S. D., Donaldson, N. R., 1987. Dynamic modelling of iceberg drift using current profiles. Fisheries and Oceans, Canada.

Sodhi, D., Dempster, R., Sep. 1975. Motion of icebergs due to changes in water currents. In: Proc. OCEAN'75. pp. 348–350.

Sodhi, D., El-Tahan, M., 1980. Prediction of an iceberg drift trajectory during a storm. Ann. Glaciol 1, 77–82.

Tenny, M., Rawlings, J., May 8–10 2002. Efficient moving horizon estimation and nonlinear model predictive control. In: Proc. American Control Conference'02. Vol. 6. pp. 4475–4480.

Turnbull, I. D., Fournier, N., Stolwijk, M., Fosnaes, T., McGonigal, D., 2015. Operational iceberg drift forecasting in northwest greenland. Cold Regions Science and Technology 110, 1 – 18.

Wächter, A., Biegler, L. T., 2006. On the implementation of an interior-point filter line-search algorithm for large-scale nonlinear programming. Mathematical Programming 106 (1), 25–57.

Walter, E., Pronzato, L., 1997. Identification of parametric models. Communications and Control Engineering 8.

WMO, 1970. WMO sea-ice nomenclature, codes, and illustrated glossary. World Meteorological Organization Rep. 259 (Tp.145), p. 147 Geneva.

Appendix A. List of figures

List of Figures

Appendix B. List of tables

List of Tables

Highlights

- An optimization-based approach for iceberg forecast is proposed.

- An ancillary current to correct for errors in the current information is proposed.

- Different performance indices to evaluate forecast performance are introduced.

- Large improvements in short-term forecast shown on two iceberg drift trajectories.

- Superior to previous solution based on adjustments of the drag coefficients.